Journal of Alloys and Compounds 505 (2010) L6–L9

Contents lists available at ScienceDirect

Journal of Alloys and Compounds

journal homepage: www.elsevier.com/locate/jallcom

Letter

Examination of $CeFe_4Sb_{12}$ upon exposure to air: Is this material appropriate for use in terrestrial, high-temperature thermoelectric devices?

Alina C. Sklad, Michael W. Gaultois, Andrew P. Grosvenor*

Department of Chemistry, University of Saskatchewan, Saskatoon, Saskatchewan, S7N 5C9, Canada

ARTICLE INFO

Article history:
Received 15 April 2010
Received in revised form 23 May 2010
Accepted 31 May 2010
Available online 11 June 2010

Keywords:
Thermoelectric materials
Oxidation
Thermal analysis
X-ray diffraction
XANES

ABSTRACT

The rare-earth (RE) filled skutterudites (*e.g.*, $CeFe_4Sb_{12}$) have been proposed for use in the next-generation of high-temperature thermoelectric devices. In this investigation, the influence of air exposure on the stability of $CeFe_4Sb_{12}$ has been studied for temperatures ranging from 300 K to 1073 K. Examination of the material after exposure to air at these temperatures using thermogravimetric analysis, powder X-ray diffraction, and X-ray absorption near-edge spectroscopy has shown that above 573 K, $CeFe_4Sb_{12}$ decomposes and then rapidly oxidizes. This temperature is much lower than the maximum operating temperature proposed for high-temperature thermoelectric devices used to recover the waste heat from vehicle exhaust systems (700–773 K).

1. Introduction

With the increasing concern of depleting fossil fuel supplies, new technologies are being actively investigated to increase the fuel efficiency of vehicles. One suggestion has been to convert the waste heat generated by exhaust systems to electricity using thermoelectric devices to power various vehicle functions [1–7]. (This technology has also been examined for the production of electricity using waste heat from power facilities and manufacturing plants [4,6].) To operate over a wide temperature range, coupled p- and n-type materials containing low-temperature (*e.g.*, Bi_2Te_3) and high-temperature (*e.g.*, rare-earth filled skutterudites; $CeFe_{1-x}Co_xSb_{12}$) thermoelectric compounds have been proposed [1,3,8]. The rare-earth filled skutterudites have become popular as candidate materials for terrestrial, high-temperature thermoelectric applications and have also been investigated for the next-generation of radioisotopic thermoelectric generators for deep-space applications (previous incarnations have already been used for >30 years) [1,3,4,7,8]. For the applications listed above, skutterudite materials may experience a considerable temperature range and it is important to understand the stability of these materials under operating conditions [3].

These rare-earth (RE) filled skutterudites have a cubic structure, which is related to that of the parent mineral, $CoAs_3$ [9]. The structure consists of a network of tilted corner-sharing metal-centred octahedra forming square Pn_4 (Pn = pnicogen = P, As, Sb) rings which, per unit cell, leads to the development of two dodecahedral cages of Pn atoms. When the transition-metal (M) has a charge of 2+ (*e.g.*, $M = Fe^{2+}$, Ru^{2+}, Os^{2+}), a RE^{3+} atom (*e.g.*, La^{3+}, Ce^{3+}, Pr^{3+}, Nd^{3+}, etc.) can occupy the dodecahedral cage, leading to materials having the empirical formula $RE^{3+}M^{2+}{}_4Pn^{1-}{}_{12}$ [10–12]. (The Pn atoms have a 1− charge because of Pn–Pn bonding.) These RE-filled skutterudite materials are described as "phonon-glass, electron-crystals" as they have low thermal conductivity but significant electrical conductivity, with most materials being metallic or small band-gap semiconductors [13,14]. The semiconducting materials are good high-temperature thermoelectrics because the RE atom can "rattle" in the dodecahedral cage of Pn atoms [5,14]. This "rattling" behaviour results in phonon scattering, which reduces the lattice thermal conductivity of the material [5,14].

Bismuth telluride and silicon–germanium alloy-based thermoelectric devices, among others, are already being successfully used for low temperature applications, while RE-filled skutterudite based systems, for high-temperature applications, are still in the development phase [1,4,8]. The proposed maximum operating temperature of $CeFe_{4-x}Co_xSb_{12}$ containing thermoelectric devices for automotive applications has been suggested to be ~700–773 K, which is below the decomposition temperature of such materials, as determined under inert atmosphere [1,3,15,16]. However, it is unknown if the decomposition temperature and reactivity of the material varies if exposed to the atmosphere. In this study, the decomposition and subsequent oxidation of $CeFe_4Sb_{12}$ upon exposure to air has been studied by thermogravimetric analysis (TGA), powder X-ray diffraction (pXRD), and X-ray absorption

* Corresponding author. Tel.: +1 306 966 4660; fax: +1 306 966 4730.
E-mail address: andrew.grosvenor@usask.ca (A.P. Grosvenor).

0925-8388/$ – see front matter © 2010 Elsevier B.V. All rights reserved.
doi:10.1016/j.jallcom.2010.05.167

near-edge spectroscopy (XANES) over a broad temperature range (300–1073 K) to investigate the suitability of using RE-filled skutterudite materials for terrestrial, high-temperature thermoelectric devices.

2. Experimental methods

2.1. Synthesis

$CeFe_4Sb_{12}$ was synthesized by combining stoichiometric amounts of the elements (Ce, HEFA Rare-earth Canada, 99.9%; Fe, Alfa Aesar, >99.9%; Sb, Alfa Aesar, 99.5%) and heating them in an evacuated C-coated fused-silica ampoule. The heating profile used to synthesize this material was similar to that reported previously [13]. To act as a standard, $FeSbO_4$ was synthesized by mixing stoichiometric amounts of Fe_2O_3 (Alfa Aesar, 99.945%) and Sb_2O_3 (Alfa Aesar, 99%), and heating them in air at 1323 K for >70 h, producing an orange powder [17]. The purity of the synthesized materials was confirmed by powder X-ray diffraction (pXRD) using a Rigaku Rotaflex RU-200 rotating anode X-ray diffractometer. $FeSbO_4$ was phase-pure while $CeFe_4Sb_{12}$ was found to contain a minor concentration of the commonly observed impurity, $FeSb_2$ [12,18].

2.2. TGA and pXRD examination of the interaction of $CeFe_4Sb_{12}$ with air

The decomposition and subsequent oxidation of $CeFe_4Sb_{12}$ in air was investigated using a TA Instruments Q5000 thermogravimetric analyser (TGA). A finely powdered sample of $CeFe_4Sb_{12}$ was heated in air (flow rate = 25 mL/min) in a Pt pan from 300 K to 1073 K at 10 K/min with the change in mass being continuously monitored. To further investigate the decomposition and oxidation of this material, aliquots of $CeFe_4Sb_{12}$ powder were heated for 2 h at temperatures ranging from 473 K to 1073 K and examined by pXRD using the previously described Rigaku instrument.

2.3. XANES

The decomposition and oxidation of $CeFe_4Sb_{12}$ initially leads to a mostly amorphous state, requiring techniques other than pXRD to study the reaction. To accomplish this, X-ray absorption near-edge spectroscopy (XANES) was used to examine the materials exposed to air for 2 h at various temperatures. XANES spectra of the Ce L_3-, Fe K-, and Sb L_3-edges were collected using beamlines located at the Canadian Light Source (CLS) and the Advanced Photon Source (APS). Using the CLS, Ce L_3- and Sb L_3-edge spectra were collected on the Soft X-ray Microcharacterization beamline (SXRMB; 06B1-1) and Fe K-edge spectra were collected on the Hard X-ray Microanalysis (HXMA; 06ID-1) beamline. Ce L_3-, Fe K-, and Sb L_3-edge spectra were also collected using the Pacific Northwest Consortium/X-ray Science Division Collaborative Access Team (PNC/XSD-CAT, Sector 20) bending magnet beamline (20BM) located at the APS, Argonne National Laboratory. Total electron yield (TEY) spectra were collected using SXRMB while fluorescence spectra, using Ge detectors, and transmission spectra, using N_2-filled ionization chambers, were collected on the HXMA and PNC/XSD-CAT beamlines. Comparison of spectra collected on different beamlines confirmed that the results are consistent regardless of detection type. Fe K-edge spectra were calibrated by setting the peak maximum of the first derivative spectrum from Fe powder or foil to 7112.0 eV [19]. The Sb L_3-edge spectra were calibrated by setting the first derivative of the Sb metal spectrum to 4132.0 eV while the Ce L_3-edge spectra were calibrated using Cr metal with an edge energy of 5989.0 eV or by aligning spectra from as-synthesized $CeFe_4Sb_{12}$ collected on multiple beamlines [19]. To aid in identification of the oxidation products, spectra from $CePO_4$ (Alfa Aesar, >99%), CeO_2 (Alfa Aesar, 99.9%), Fe_2O_3, $FeSbO_4$, Sb_2O_3, and Sb_2O_5 (Alfa Aesar, 99.998%) were also collected. All spectra were analyzed using the Athena software program [20].

3. Results

3.1. TGA

A plot of the increase in mass, in percent, experienced by powdered $CeFe_4Sb_{12}$ when heated from ~300 K to 1073 K in air, as determined by TGA, is presented in Fig. 1. As the temperature increases through, and above 573 K, the mass of the material increases significantly. The numerous changes in slope observed in the profile imply multiple oxidation events.

3.2. pXRD

To understand the effect of exposing $CeFe_4Sb_{12}$ to air, samples of this material were heated in air for 2 h at 473 K, 573 K, 673 K, 773 K, and 1073 K and examined by pXRD. The surface of the material

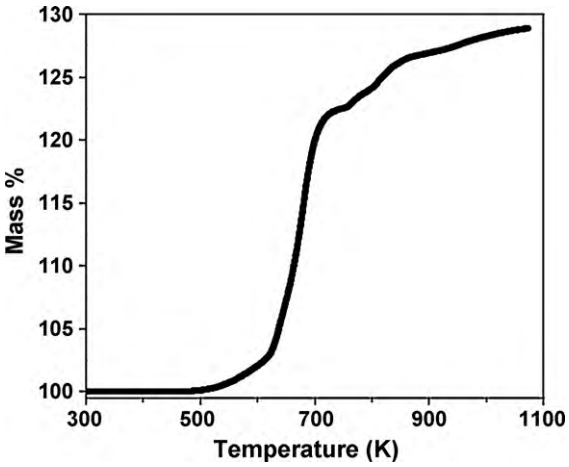

Fig. 1. TGA profile from $CeFe_4Sb_{12}$ heated in air from 300 K to 1073 K.

was dark grey in colour below 473 K, blue after being held in air at 573 K, and orange/brown above this temperature. Powder XRD patterns collected from samples heated in air at 573 K, 673K, 773 K, and 1073 K are presented in Fig. 2. (Peaks representing identified phases are labelled with symbols.)

Below 573 K, the powder XRD patterns show that the primary phase present is ordered $CeFe_4Sb_{12}$ (Fig. 2a). After heating in air at 673 K (Fig. 2b) for 2 h, $CeFe_4Sb_{12}$ was no longer observed, and the few intense peaks present correspond to the formation of ordered Ce_7O_{12}, with no peaks from Fe or Sb species being found. At 773 K (Fig. 2c), Ce_7O_{12} and Sb_2O_4 were observed with no evidence of

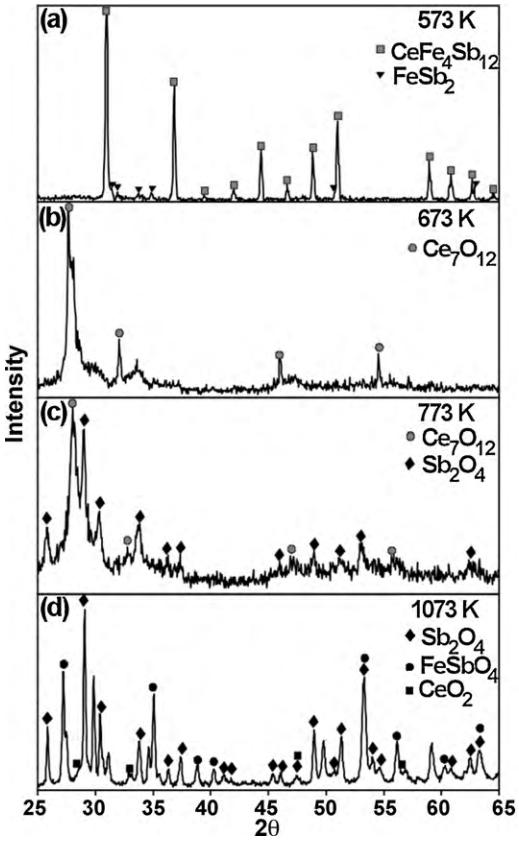

Fig. 2. Powder XRD patterns from $CeFe_4Sb_{12}$ after exposure to air for 2 h at 573 K (a), 673 K (b), 773 K (c), and 1073 K (d). Peaks corresponding to known phases have been labelled using symbols. The unlabelled peaks found in (d) represent an unidentified Ce-containing phase.

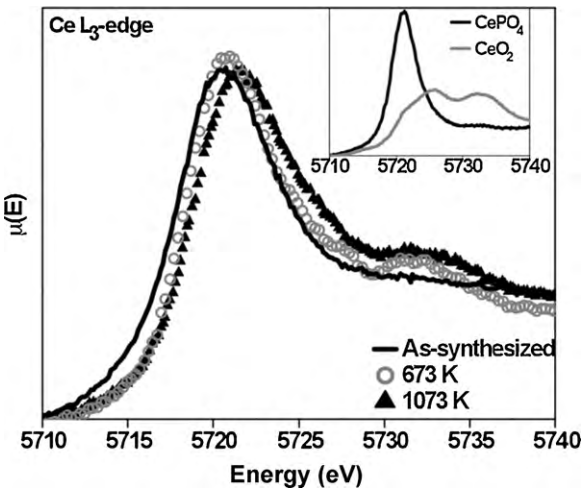

Fig. 3. Normalized Ce L_3-edge XANES spectra from $CeFe_4Sb_{12}$ exposed to air at room temperature (as-synthesized), 673 K, and 1073 K. For comparison purposes, Ce L_3-edge spectra from $CePO_4$ and CeO_2 are presented in the inset.

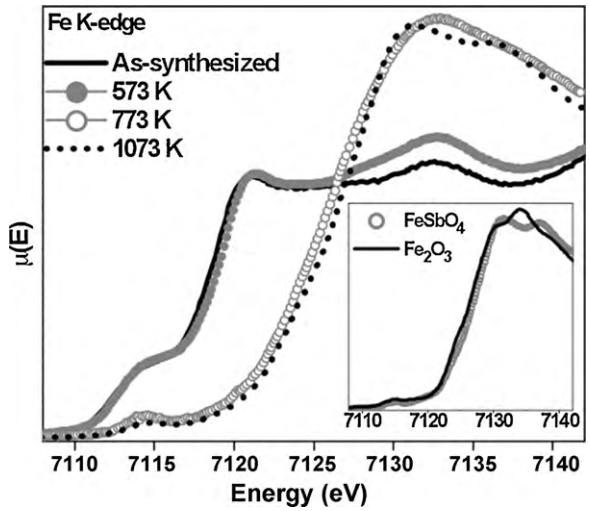

Fig. 4. Normalized Fe K-edge spectra from $CeFe_4Sb_{12}$ exposed to air at room temperature, 573 K, 773 K, and 1073 K. Spectra from Fe_2O_3 and $FeSbO_4$ are presented in the inset.

ordered Fe-bearing phases. After exposure to air at 1073 K (Fig. 2d), $CeFe_4Sb_{12}$ was converted to Sb_2O_4 and $FeSbO_4$, a minor quantity of CeO_2, and an unidentified phase.

3.3. XANES

Below 1073 K, pXRD analysis shows the formation of ordered oxides containing only some of the elements present in $CeFe_4Sb_{12}$. This observation implies that amorphous oxides containing the missing elements must also be present. To further examine the amorphous and ordered oxides formed, XANES was performed.

3.3.1. Ce L_3-edge XANES spectra

The Ce L_3-edge XANES spectra, resulting from a Ce 2p → Ce 4d transition, are presented in Fig. 3 for as-synthesized $CeFe_4Sb_{12}$ (*i.e.*, before exposure to air above room temperature) and $CeFe_4Sb_{12}$ after exposure to air at 673 K, and 1073 K [21]. For comparison, spectra from $CePO_4$ (Ce^{3+}) and CeO_2 (Ce^{4+}) are shown in the inset. The spectrum from as-synthesized $CeFe_4Sb_{12}$ is characteristic of Ce^{3+} (*cf.*, $CePO_4$ in Fig. 3). This lineshape was generally conserved for samples of $CeFe_4Sb_{12}$ exposed to air at 473 K and 573 K (not shown).

After heating in air at 673 K, the Ce L_3-edge spectrum shows a main signal whose peak maximum is centred at 5720.8 eV (indicative of Ce^{3+}) and is slightly broader than the corresponding peak from $CeFe_4Sb_{12}$ heated at ≤573 K. A second peak is observed at ~5732 eV, which, as can be seen by examining the spectrum from CeO_2 (inset of Fig. 3), is representative of the formation of Ce^{4+}. The observation of both Ce^{3+} and Ce^{4+} agrees with the identification of Ce_7O_{12} (average Ce charge of ~3.4+) by pXRD (Fig. 2b). Note that the intense Ce^{3+} peak observed in this spectrum (Fig. 3) is shifted to slightly higher energy than that found for as-synthesized $CeFe_4Sb_{12}$ (5720.5 eV). This is a result of the decreased screening of the Ce nuclear charge experienced when it is bound to O, which is more electronegative than Sb. Upon exposure of $CeFe_4Sb_{12}$ to air at 1073 K, the Ce L_3-edge spectrum (Fig. 3) has a broader low-energy peak (5721.4 eV), and a more intense high-energy peak (~5732 eV) than materials oxidized at lower temperatures. This suggests that the Ce oxide formed at this temperature contains more Ce^{4+} than is present in Ce_7O_{12}.

3.3.2. Fe K-edge XANES spectra

Fe K-edge XANES spectra from as-synthesized $CeFe_4Sb_{12}$ as well as samples exposed to air at temperatures ranging from 573 K to 1073 K are presented in Fig. 4. For comparison, spectra from Fe_2O_3 and $FeSbO_4$ are shown in the inset. The spectrum from as-synthesized $CeFe_4Sb_{12}$ is comprised of 3 main excitations and corresponds to low-spin Fe^{2+}, an electronic state that has been proven by previous studies [18,22]. The lowest energy peak in the spectrum (~7114 eV) represents a pre-edge, Fe 1s → Fe 3d, excitation. Based on comparison to spectra from other transition-metal pnictides, the slightly higher energy peak (~7121 eV) represents a Fe 1s → Sb 5p excitation, which is followed by a peak at higher energy (~7133 eV) corresponding to a Fe 1s → Fe 4p excitation [23].

No change was observed in the Fe K-edge spectra until the material was exposed to air at 573 K, at which point an increase in intensity of the peak located at ~7133 eV was observed (Fig. 4). Comparison to the spectrum from Fe_2O_3 (inset of Fig. 4) implies that the growth of this peak corresponds to the formation of an Fe^{3+} oxide. This phase is amorphous as no Fe-oxide peaks were identified by pXRD, and its presence is confirmed by the TGA results (Fig. 1), which show an increase in mass near 573 K. With increasing temperature, the Fe K-edge spectra (Fig. 4) show no presence of $CeFe_4Sb_{12}$ and instead resemble Fe^{3+} oxides with spectra having similar lineshapes to Fe_2O_3 when the oxidation temperature was ≤773 K or $FeSbO_4$ when the materials were exposed to a higher temperature (*e.g.*, 1073 K).

3.3.3. Sb L_3-edge XANES spectra

The Sb L_3-edge spectra (Sb 2p → Sb 4d/5s excitation) from $CeFe_4Sb_{12}$ exposed to air at various temperatures are presented in Fig. 5. Standard spectra from Sb_2O_3, Sb_2O_5, and $FeSbO_4$ are shown in the inset. The energy of the peak maximum from the first derivative spectrum from as-synthesized $CeFe_4Sb_{12}$ (4131.0 eV) is lower than for Sb metal (4132.0 eV), in agreement with the charge assignment of 1−. After exposure to air at 673 K, the lineshape and energy of the spectrum is similar to that from Sb_2O_3 and Sb_2O_5. This indicates the formation of an amorphous oxide, as no Sb oxides were detected by pXRD. When exposed to air at 773 K, the similarity of the spectra (not shown) to those from Sb_2O_3 and Sb_2O_5 is in agreement with the observation of Sb_2O_4 (containing Sb^{3+} and Sb^{5+}) in the corresponding pXRD pattern (Fig. 2c). After exposure of $CeFe_4Sb_{12}$ to air at 1073 K, the Sb L_3-edge XANES spectrum compares very well to that from $FeSbO_4$ (inset of Fig. 5).

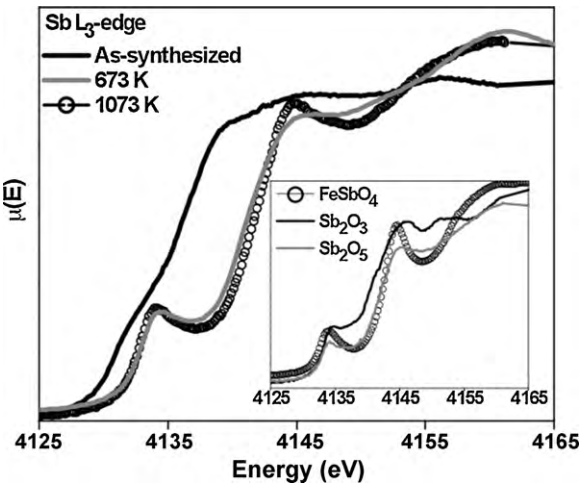

Fig. 5. Normalized Sb L_3-edge spectra from $CeFe_4Sb_{12}$ after exposure to air at various temperatures. To aid in the interpretation of these spectra, spectra from Sb_2O_3, S_2O_5, and $FeSbO_4$ are presented in the inset.

4. Discussion

The above results show that although $CeFe_4Sb_{12}$ is stable in an inert environment at temperatures above the proposed maximum operating temperature of thermoelectric devices for automotive applications (~700–773 K), upon exposure to air, the temperature at which the material decomposes and subsequently oxidizes is significantly reduced (~573 K). Examination of $CeFe_4Sb_{12}$ after exposure to air by TGA, pXRD, and XANES indicated that above ~573 K, powdered $Ce^{3+}Fe^{2+}{}_4Sb^{1-}{}_{12}$ completely decomposed and oxidized, leading to the formation of amorphous Fe^{3+} and $Sb^{3+/5+}$ oxides along with ordered Ce_7O_{12}, a low-temperature stable Ce oxide phase [24]. The absence of any phases containing Fe–Sb, Sb–Sb, or Ce–Sb bonds indicates that all of these bonds, which are present in the parent material, are broken above 573 K due to a greater preference for forming Fe–O, Sb–O, and Ce–O bonds.

With increasing oxidation temperature (>573 K), ordered Ce and Sb oxides (Ce_7O_{12} and Sb_2O_4) were observed while the Fe^{3+} oxide phases present were amorphous. After being exposed to air at 1073 K, which is well above the decomposition temperature of $CeFe_4Sb_{12}$ in an inert environment, $CeFe_4Sb_{12}$ was converted to Sb_2O_4, $FeSbO_4$, CeO_2 (minor amount) and a Ce oxide whose structure is not known [14,15]. As the Ce L_3-edge XANES spectrum (Fig. 3) indicated the presence of Ce^{3+} and Ce^{4+}, the unidentified Ce oxide is likely an oxygen-deficient phase of CeO_2 (i.e., CeO_{2-x}) formed through the dissociation of Ce_7O_{12} [24]. The unidentified peaks observed in the corresponding pXRD pattern (Fig. 2d) are suspected to belong to this oxygen deficient Ce oxide. The observation of $FeSbO_4$ after exposure of $CeFe_4Sb_{12}$ to air at 1073 K by pXRD (Fig. 2), and Fe K- and Sb L_3-edge XANES (Figs. 4 and 5), is consistent with the synthesis of this oxide (see Section 2.1 and Ref. [17]).

5. Conclusions

The decomposition and subsequent oxidation of $CeFe_4Sb_{12}$ in air has been studied for the temperature range of 300–1073 K by TGA, pXRD, and XANES. This study has shown that, when exposed to the atmosphere, $CeFe_4Sb_{12}$ decomposes and then oxidizes above 573 K. To be used in thermoelectric devices that will be exposed to air, this material will need to be protected. To limit its exposure to the atmosphere, $CeFe_4Sb_{12}$ could be sealed in an inert environment, as has been done for other thermoelectric materials [1]. Manufacturing the device to operate using large, dense thermoelectric segments (*e.g.*, 40 mm diameter disks of skutterudites have been produced) may also have a positive affect on the stability of this material [4]. Increasing the dimensions of the thermoelectric segment will reduce the surface area to volume ratio of the material which, as has been shown for $CoAs_3$, will minimize the ability of $O_{2(g)}$ to interact with $CeFe_4Sb_{12}$; elevating its decomposition and oxidation temperatures [25]. Noting this, any surface decomposition and oxidation may degrade the connections between materials, leading to device failure. Although the RE-filled skutterudites have deep-space applications, this investigation has shown that, unless well protected, the usefulness of these materials for terrestrial, high-temperature applications appears limited.

Acknowledgements

The University of Saskatchewan is thanked for supporting this research through a new-faculty start-up grant to APG. Dr. Robert Scott (Department of Chemistry, University of Saskatchewan) is thanked for providing access to the TGA. Dr. Yongfeng Hu and Dr. Ning Chen are thanked for help in carrying out XANES measurements at 06B1-1 and 06ID-1 at the CLS. The Canadian Light Source is supported by NSERC, NRC, CIHR, and the University of Saskatchewan. Dr. Robert Gordon is thanked for help in carrying out XANES experiments at PNC/XSD-CAT, sector 20 at the APS. PNC/XOR facilities at the Advanced Photon Source, and research at these facilities, are supported by the US Department of Energy-Basic Energy Sciences, a Major Research Support (MRS) grant from NSERC, the University of Washington, Simon Fraser University, and the Advanced Photon Source. Use of the Advanced Photon Source is also supported by the U.S. Department of Energy, Office of Science, Office of Basic Energy Sciences, under contract DE-AC02-06CH11357.

References

[1] J. Yang, T. Caillat, MRS Bull. 31 (2006) 224–229.
[2] T. Kajikawa, J. Electron. Mater. 38 (2009) 1083–1088.
[3] T. Kajikawa, M. Ozaki, K. Yamaguchi, H. Obara, 24th International Conference on Thermoelectrics, 2005, pp. 147–154.
[4] J.-P. Fleurial, JOM 61 (2009) 79–85.
[5] G.S. Nolas, D.T. Morellie, T.M. Tritt, Annu. Rev. Mater. Sci. 29 (1999) 89–116.
[6] C.B. Vining, Nat. Mater. 8 (2009) 83–85.
[7] B.C. Sales, in: K.A. Gschneidner, J.-C. Bunzli, V.K. Pecharsky (Eds.), Handbook on the Physics and Chemistry of Rare Earths, vol. 33, Elsevier, Amsterdam, 2003, pp. 1–34.
[8] V. Ravi, S. Firdosy, T. Caillat, E. Brandon, K. van der Walder, L. Maricic, A. Sayir, J. Electron. Mater. 38 (2009) 1433–1442.
[9] S. Rundqvist, N.-O. Ersson, Ark. Kemi 30 (1968) 103–114.
[10] W. Jeitschko, D. Braun, Acta Crystallogr. Sect. B: Struct. Crystallogr. Cryst. Chem. 33 (1977) 3401–3406.
[11] D.J. Braun, W. Jeitschko, J. Solid State Chem. 32 (1980) 357–363.
[12] D.J. Braun, W. Jeitschko, J. Less-Common Met. 72 (1980) 147–156.
[13] B.C. Sales, D. Mandrus, B.C. Chakoumakos, V. Keppens, J.R. Thompson, Phys. Rev. B 56 (1997) 15081–15089.
[14] G.A. Slack, in: D.M. Rowe (Ed.), CRC Handbook of Thermoelectrics, CRC Press, Boca Raton, FL, 1995, pp. 407–440.
[15] M.D. Hornbostel, E.J. Hyer, J.H. Edvalson, D.C. Johnson, Inorg. Chem. 36 (1997) 4270–4274.
[16] S.R. Brown, S.M. Kauzalarich, F. Gascoin, G.J. Snyder, Chem. Mater. 18 (2006) 1873–1877.
[17] J. Walczak, E. Filipek, M. Bosacka, Solid State Ionics 101–103 (1997) 1363–1367.
[18] A.P. Grosvenor, R.G. Cavell, A. Mar, Phys. Rev. B 74 (2006), 125102/1-10.
[19] A. Thompson, D. Attwood, E. Gullikson, M. Howells, K.-J. Kim, J. Kirz, J. Kortright, I. Lindau, P. Peanetta, A. Robinson, J. Scofield, J. Underwood, D. Vaughan, G. Williams, H. Winick, X-ray Data Booklet, Lawrence Berkeley National Laboratory, University of California, Berkeley, 2001.
[20] B. Ravel, M. Newville, J. Synchrotron Rad. 12 (2005) 537–541.
[21] C.H. Lee, H. Oyanagi, C. Sekine, I. Shirotani, M. Ishii, Phys. Rev. B 60 (1999) 13253–13256.
[22] F. Grandjean, A. Gérard, D.J. Braun, W. Jeitschko, J. Phys. Chem. Solids 45 (1984) 877–886.
[23] A.P. Grosvenor, R.G. Cavell, A. Mar, J. Solid State Chem. 180 (2007) 2702–2712.
[24] G. Adachi, N. Imanaka, Chem. Rev. 98 (1998) 1479–1514.
[25] L.J. Wilson, S.A. Mikhail, Thermochim. Acta 156 (1989) 107–115.